

Emergent Berezinskii-Kosterlitz-Thouless and Kugel-Khomskii physics in the triangular lattice bilayer colbaltate

Gang V. Chen*

International Center for Quantum Materials, School of Physics, Peking University, Beijing 100871, China and Collaborative Innovation Center of Quantum Matter, 100871, Beijing, China

Motivated by the experiments on the triangular lattice bilayer colbaltate $\text{K}_2\text{Co}_2(\text{SeO}_3)_3$, we formulate a theory to explore the underlying physics from a couple observation. The model is composed of interacting Co^{2+} dimers on the triangular lattice, where the Co^{2+} ion provides an effective spin-1/2 local moment via the spin-orbit coupling and the crystal field effect. The intra-dimer interaction is dominant and would simply favor the local spin singlet, and the inter-dimer interactions compete with the inter-dimer interaction, leading to rich behaviors. With the easy-axis anisotropy, it is shown that, in the ground state manifold of the intra-dimer Ising interaction, the system realizes an effective transverse field Ising model, where the ground state is either a three-sublattice order or Ising disordered. The finite temperature regime naturally realizes the Berezinskii-Kosterlitz-Thouless physics. To explore the full excitations, we incorporate the excited state manifold of the intra-dimer Ising interaction and establish the emergent Kugel-Khomskii physics. Thus, the triangular lattice bilayer colbaltate is an excellent platform to explore the interplay between geometrical frustration and anisotropic interactions as well as the emergent effective models and the resulting physics.

Frustrated magnets have been an active field in modern condensed matter physics [1]. Frustration arises from competing interaction that cannot be optimized simultaneously. A common source of frustration is the geometrical frustration on frustrated lattices such as triangular, kagomé, and pyrochlore lattices. The study of frustrated magnets on these frustrated lattices has contributed to a large portion of topics. Theoretically, frustration generates a large number of degenerate and nearly degenerate many-body states on which the sub-dominant interactions are reduced to effective interaction and then lead to rather interesting and exotic behaviors. Thus, the ingredient of frustration has inspired many contrived theoretical models and works in last two decades. On the other hand, the abundance of frustrated magnetic materials has provided the experimental motivation for new frustrated models and phenomena out of the frustration.

One ongoing interest on the frustrated materials is about the spin-orbit-coupled Mott insulators [2]. These materials are often the $4d/5d$ transition metal compounds and $4f$ rare-earth magnets. In these systems, due to the spin-orbit coupling and the electron correlation, the magnetic interactions are often quite anisotropic, both in the spin space and the position space. The resulting models may often differ significantly from simple Heisenberg models, and these anisotropic models may carry strong frustration even on unfrustrated lattices. The representative example is the honeycomb lattice Kitaev model that has the relevance on various iridates and $\alpha\text{-RuCl}_3$ [3]. With both anisotropy and frustration, it is natural to expect that these anisotropic and frustrated models on geometrically frustrated lattices could bring more unexpected behaviors. Much progress has been made in the rare-earth pyrochlore magnets [4] and the

$4d/5d$ Kitaev materials [3].

Some of the recent attention has been directed to the colbaltates. One motivation was to explore the Kitaev interaction and Kitaev spin liquid physics among the honeycomb colbaltates where the spin-orbit coupling plays a similar role as the one for the iridates and induces the anisotropic interactions, and the progress has been made in the honeycomb magnets $\text{Na}_2\text{Co}_2\text{TeO}_6$ and $\text{Na}_3\text{Co}_2\text{SbO}_6$ [5, 6]. In fact, the spin-orbit coupling can sometimes play an important role for the underlying physics even in the $3d$ transition metal compounds, and this differs from elements to elements and also depends on the crystal environments. Moreover, several colbaltates are long known to be good realizations of the anisotropic models such as the quantum Ising model as the extreme limit. These include the quasi-1D Ising magnets CoNb_2O_6 [7–9], $\text{BaCo}_2\text{V}_2\text{O}_8$ [10–12], and $\text{SrCo}_2\text{V}_2\text{O}_8$ [13] where not only the external field gives a useful tunability of the quantum phases but also the system could produce emergent and exotic excitations associated with the criticality [14].

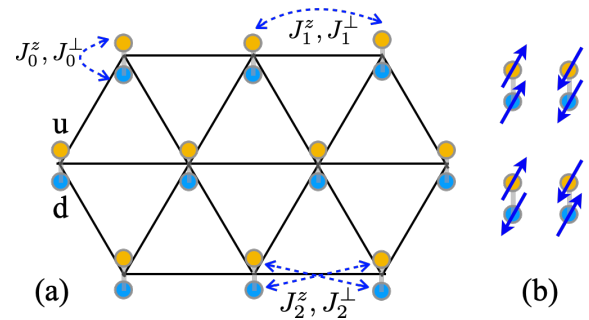


FIG. 1. (a) The dimers of the Co^{2+} ions form a triangular lattice. (b) Two anticollinear and two collinear spin configurations on the dimer, where the spins point along the $\pm\hat{z}$ direction.

* Away from University of Hong Kong

S_{ui}^z	S_{ui}^x	S_{ui}^y	S_{di}^z	S_{di}^x	S_{di}^y	$S_{ui}^z S_{di}^z$	$S_{ui}^x S_{di}^x + S_{ui}^y S_{di}^y$
τ_i^z	0	0	$-\tau_i^z$	0	0	$-\frac{1}{4}$	τ_i^x
τ_i^z	$2\tau_i^x \mu_i^x$	$2\tau_i^y \mu_i^x$	$2\tau_i^z \mu_i^z$	μ_i^x	$2\tau_i^z \mu_i^y$	$\frac{\mu_i^z}{2}$	$\tau_i^x (\frac{1}{2} - \mu_i^z)$

TABLE I. The list of spin operators on each dimer under different representations. The first line is the original spin operator on the local lattice site. The second line is in terms of the pseudospin τ_i^μ after being projected onto the ground state manifold of the intra-dimer Ising interaction. The third line is in terms of the pseudospin τ_i^μ and μ_i^ν after including all the local states of the dimer. The prescription is described in the main text.

We are inspired by the experiments on the Co-dimer triangular lattice antiferromagnet $\text{K}_2\text{Co}_2(\text{SeO}_3)_3$ [15]. As it is shown in Fig. 1, the two neighboring Co^{2+} ions form a dimer along z direction, and these dimers are then organized into a triangular lattice. It can be equivalently viewed as a bilayer triangular lattice, and the interlayer separation is quite short compared to the lattice constant. The magnetic susceptibility and the magnetization measurements clearly indicate the easy-axis spin anisotropy, and the magnetic entropy is consistent with the effective spin-1/2 degree of freedom for each Co^{2+} ion. The presence of the 1/3 magnetization plateau is compatible with the predominant Ising interaction or Ising-like magnetic moments. Given the previous success of the triangular lattice XXZ model on the spin supersolid compound $\text{Na}_2\text{BaCo}(\text{PO}_4)_2$ [16–18] and the 120-degree ordered compound $\text{Ba}_3\text{CoSb}_2\text{O}_9$ [19], we consider an extended XXZ model with the easy-axis anisotropy on this bilayer triangular lattice. In the absence of the magnetic field, the intra-dimer Ising interaction favors the anticollinear spin configuration. Within this manifold, we show that the remaining interactions effectively realize a quantum Ising model on the triangular lattice and then gives rise to the quantum order by disorder effect and the Berezinskii-Kosterlitz-Thouless (BKT) physics at finite temperatures. Although the original XXZ model has a $U(1)$ symmetry, the emergent BKT physics has no connection with the $U(1)$ spin symmetry of the spin model. For the magnetic excitations and the magnetization plateau states, the states out of the intra-dimer anticollinear spin states are naturally involved. After incorporating these “excited” collinear states in Fig. 1(b), we end up with the Kugel-Khomskii-like model and thus deal with the Kugel-Khomskii (KK) physics.

To explore the interesting interplay between geometrical frustration and anisotropic interaction, we first write down the extended XXZ model with the spin-1/2 moments on the dimer triangular lattice,

$$H = H_0 + H_u + H_d + H_{ud} + H_Z, \quad (1)$$

where the five different terms are given as

$$H_0 = \sum_i [J_0^z S_{ui}^z S_{di}^z + J_0^\perp (S_{ui}^x S_{di}^x + S_{ui}^y S_{di}^y)], \quad (2)$$

$$H_u = \sum_{\langle ij \rangle} [J_1^z S_{ui}^z S_{uj}^z + J_1^\perp (S_{ui}^x S_{uj}^x + S_{ui}^y S_{uj}^y)], \quad (3)$$

$$H_d = \sum_{\langle ij \rangle} [J_1^z S_{di}^z S_{dj}^z + J_1^\perp (S_{di}^x S_{dj}^x + S_{di}^y S_{dj}^y)], \quad (4)$$

$$H_{ud} = \sum_{\langle ij \rangle} [J_2^z S_{ui}^z S_{dj}^z + J_2^\perp (S_{ui}^x S_{dj}^x + S_{ui}^y S_{dj}^y)] \\ + [J_2^z S_{di}^z S_{uj}^z + J_2^\perp (S_{di}^x S_{uj}^x + S_{di}^y S_{uj}^y)], \quad (5)$$

$$H_Z = \sum_i -B(S_{ui}^z + S_{di}^z). \quad (6)$$

Here H_0 is the intra-dimer interaction, H_u is the inter-dimer interaction within the up layer, H_d is the inter-dimer interaction within the down layer, H_{ud} is the inter-dimer interaction between the up and down layers, and H_Z is the Zeeman coupling for the field along the z direction. The spin operator S_{ui}^μ (S_{di}^μ) refers to the spin component μ at the lattice site i from the up (down) layer of the dimer triangular lattice. The spin interactions are labeled in Fig. 1(a).

From the lattice geometry, the intra-dimer interaction should be dominant. From the easy-axis anisotropy, the intra-dimer Ising interaction J_0^z is stronger than the xy exchange J_0^\perp . Thus, throughout this work, we will treat the intra-dimer Ising interaction as the dominant interaction. For the inter-dimer interaction, we still consider the easy-axis anisotropy. Moreover, we expect $J_1^z \gg J_2^z$ from the different exchange paths.

We consider the zero-field case. The ground states of the intra-dimer Ising interaction are doubly degenerate for each dimer, and we introduce an effective pseudospin-1/2 states to label them as

$$|\tau_i^z = +\frac{1}{2}\rangle = |S_{ui}^z = +\frac{1}{2}, S_{di}^z = -\frac{1}{2}\rangle, \quad (7)$$

$$|\tau_i^z = -\frac{1}{2}\rangle = |S_{ui}^z = -\frac{1}{2}, S_{di}^z = +\frac{1}{2}\rangle. \quad (8)$$

We define a projection operator to this reduced local Hilbert space, $P = \prod_i \sum_\alpha |\tau_i^z = \alpha\rangle \langle \tau_i^z = \alpha|$. The effective model in this reduced Hilbert space is $H_{\text{eff}} = PHP$. Different spin operators in this reduced Hilbert space is expressed in Tab. I. The effective model is given as a

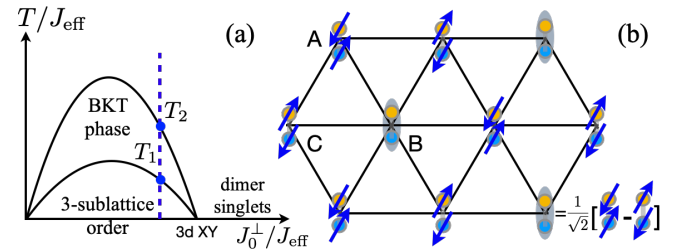


FIG. 2. (a) The phase diagram of quantum Ising model (adapted from Ref. 20), where $J_{\text{eff}} = 2(J_1^z - J_2^z)$. (b) The three-sublattice order in the limit of weak transverse field for the dimer triangular lattice.

transverse field Ising models with

$$H_{\text{eff}} = \sum_i J_0^\perp \tau_i^x + \sum_{\langle ij \rangle} 2(J_1^z - J_2^z) \tau_i^z \tau_j^z - \frac{NJ_0^z}{4}, \quad (9)$$

where N is the total number of dimers. This is a good approximation as long as J_0^z is large enough. Remarkably, the inter-dimer transverse exchanges all disappear in this projection as they do not connect the singlet manifolds of neighboring dimers. Unlike CoNb_2O_6 [7–9], $\text{BaCo}_2\text{V}_2\text{O}_8$ [10–12] whose transverse field is applied externally, the transverse field here is of the intrinsic origin [21]. From this effective model, one can obtain many properties of the system. The phase diagram of this model is well-known from Ref. 20 and is adapted to our problem in Fig. 2(a), where we set $J_{\text{eff}} = 2(J_1^z - J_2^z)$. There are two phases at zero temperature. With the large transverse field, the ground state is polarized in the negative τ^x direction, which is equivalent to the local singlet for each dimer. When the effective exchange becomes large, a three-sublattice order is favored instead, leading to the Bragg peaks at the \mathbf{K} points of the Brillouin zone. This three-sublattice order is better visualized in terms of the original spin configuration instead of the pseudospin τ_i configuration. We depict this three-sublattice spin configuration in the limit of weak transverse field. For more generic cases, τ^x is polarized by the transverse field, and thus, each dimer is a mixture of the spin singlet and the antiferromagnetic configuration. The property in this three-sublattice order can be captured by a Weiss mean-field theory (MFT) with

$$H_{\text{eff}} \rightarrow H_{\text{MF}} = \sum_i J_0^\perp \tau_i^x + \sum_{\langle ij \rangle} J_{\text{eff}} \tau_i^z \langle \tau_j^z \rangle, \quad (10)$$

where $\langle \tau_j^z \rangle$ is the mean-field order parameter for each site. The details are discussed in the appendix. The excitations are plotted in Fig. 3, and there exists a mini-gap in the spectrum. This is known as the pseudo-Goldstone mode that results from the quantum order by disorder effect. The effective model does not have the continuous symmetry and the magnetic order does not break the $U(1)$ symmetry of the original spin model in Eq. (1), so the excitation spectrum is fully gapped. The quantum correction or renormalization of the order parameter is not considered in this MFT and thus the bandwidth of the excitations is enhanced compared to the reality. Nevertheless, the overall dispersion does not significantly depend on the order parameter. The critical value of J_0^\perp/J_{eff} in the mean-field theory is 1.5 while the numerical result from quantum Monte Carlo is ~ 0.82 [22, 23]. It is important to mention that the excitations are expressed in the variable of τ_i . The τ^z - τ^z correlation should

create the magnon excitations as well as two-magnon continuum in the three-sublattice ordered states, and creates the magnon-like dispersive excitation in the Ising disordered state. The local probe such as NMR and μSR should also be useful to detect the dynamics in this reduced Hilbert space. The τ^x component is the bond operator in terms of the original spin variables and is even under time reversal. A useful probe is likely to be the X-ray pair distribution function measurement.

At finite temperatures above the three-sublattice order, the order melts via the two-step process before entering the high-temperature paramagnet (see Fig. 2(a)) [20, 24]. The two finite-temperature phase transitions are of the BKT type, and the precise locations of the transitions, T_1 and T_2 (especially the higher temperature one), might be a bit difficult to detect experimentally and even numerically, and show up as broad peaks in specific heat. Below T_1 , the magnetic order emerges as a rigid order with a clear gap, and thus T_1 is better to be identified. Between T_1 and T_2 , the system is in a BKT phase with an emergent $U(1)$ symmetry and the spin correlations are of the power law form. It is an algebraically ordered regime but has no true long-range order with [25]

$$\langle \tau_i^z \tau_j^z \rangle \sim \frac{\cos[\mathbf{Q} \cdot (\mathbf{r}_i - \mathbf{r}_j)]}{|\mathbf{r}_i - \mathbf{r}_j|^{\eta(T)}}, \quad (11)$$

where the wavevector \mathbf{Q} corresponds to the momentum \mathbf{K} , and $\eta \in (1/9, 1/4)$ is temperature dependent. It was even predicted that, the uniform susceptibility in τ^z is singular in the power-law in the zero-field limit if a uniform field is applied to the pseudospin τ^z components [26]. This corresponds to a weak Γ point peak in the τ^z - τ^z correlation, and it is not true ferromagnetic order in τ^z . If the system is close to the quantum phase transition between the three-sublattice order and the Ising disordered state, the system would be controlled by the critical mode at the finite temperatures, and have a T^2 specific heat.

To obtain the full excitations, we ought to return to the original spin model in Eq. (1). Without losing connection to the effective model in Eq. (9), we incorporate the local excited states in Fig. 1(b) as

$$|\tau_i^z = +\frac{1}{2}, \mu_i^z = +\frac{1}{2}\rangle = |S_{ui}^z = +\frac{1}{2}, S_{di}^z = +\frac{1}{2}\rangle, \quad (12)$$

$$|\tau_i^z = -\frac{1}{2}, \mu_i^z = +\frac{1}{2}\rangle = |S_{ui}^z = -\frac{1}{2}, S_{di}^z = -\frac{1}{2}\rangle, \quad (13)$$

and the ground states in Eq. (7) and Eq. (8) are then treated as $|\mu_i^z = -1/2\rangle$ with the same τ^z 's. In this representation of the local Hilbert space, the spin variables are re-expressed in terms of the pseudospins τ^μ and μ^ν and are listed in Tab. I. The original model in Eq. (1) now becomes

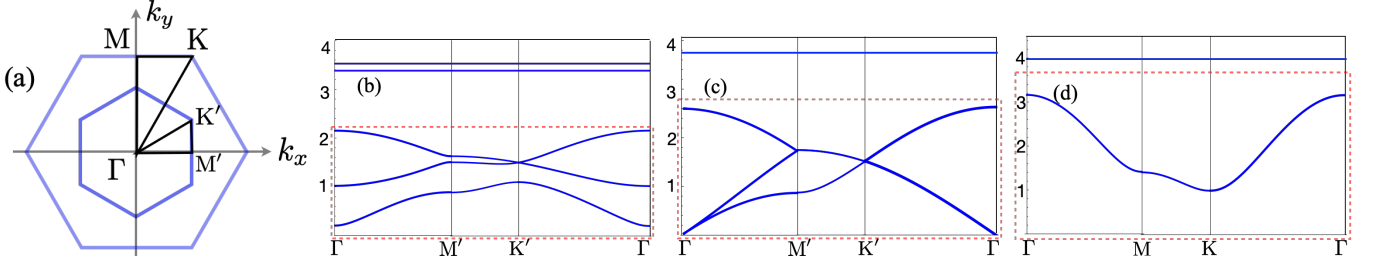


FIG. 3. The full elementary excitations in different zero-temperature phases for the minimal model H_{min} . (a) The lattice Brillouin zone and the magnetic Brillouin zone with the high symmetry momentum lines. (b) The elementary excitations in the three sublattice ordered state, where we choose $J_{\text{eff}} = 1$, $J_0^\perp = 1.1$, $J_0^z = 6$. (c) The elementary excitations in the critical state, where we choose $J_{\text{eff}} = 1$, $J_0^\perp = 1.5$, $J_0^z = 6$. (d) The elementary excitations in the Ising disordered state, where we choose $J_{\text{eff}} = 1$, $J_0^\perp = 2$, $J_0^z = 6$. The spectra in the (red) dashed box are the elementary excitations for the effective model H_{eff} , and the rest are from the μ sector.

$$\begin{aligned}
H = & \sum_i \left[\frac{1}{2} J_0^z \mu_i^z + J_0^\perp \tau_i^x \left(\frac{1}{2} - \mu_i^z \right) \right] + \sum_{\langle ij \rangle} \left[4 J_1^z \tau_i^z \tau_j^z \left(\frac{1}{4} + \mu_i^z \mu_j^z \right) + 4 J_1^\perp \left[\left(\frac{1}{4} + \tau_i^x \tau_j^x \right) \mu_i^x \mu_j^x + \tau_i^y \tau_j^y \mu_i^x \mu_j^x + \tau_i^z \tau_j^z \mu_i^y \mu_j^y \right] \right] \\
& + \sum_{\langle ij \rangle} \left[2 J_2^z \tau_i^z \tau_j^z (\mu_i^z + \mu_j^z) + 4 J_2^\perp \left[\frac{1}{2} (\tau_i^x + \tau_j^x) \mu_i^x \mu_j^x + \tau_i^y \tau_j^z \mu_i^x \mu_j^y + \tau_i^z \tau_j^y \mu_i^y \mu_j^x \right] \right] - \sum_i B \tau_i^z (1 + 2 \mu_i^z). \quad (14)
\end{aligned}$$

It is in the form of the Kugel-Khomskii model except that the local degrees of freedom are from the dimer instead of the spin and orbitals [27]. Thus, the system belongs to the so-called “multiflavor Mott insulator” [28]. Based on this model, one can proceed and calculate the full excitations of the three-sublattice order as well as the dimer singlet state. The presence of J_1^\perp , J_2^\perp couplings may generate more phases if they become comparable to the Ising exchanges. To avoid further complication, we set $J_1^\perp = J_2^\perp = 0$ as they might be weaker compared to their corresponding Ising couplings. The simplified model is the minimal model for our calculation below and is given as

$$H_{\text{min}} = \sum_i \left[\frac{1}{2} J_0^z \mu_i^z + J_0^\perp \tau_i^x \left(\frac{1}{2} - \mu_i^z \right) \right] + \sum_{\langle ij \rangle} \left[J_1^z \tau_i^z \tau_j^z (1 + 4 \mu_i^z \mu_j^z) + 2 J_2^z \tau_i^z \tau_j^z (\mu_i^z + \mu_j^z) \right] - \sum_i B \tau_i^z (1 + 2 \mu_i^z). \quad (15)$$

We would like to explain why we introduce the effective model first and then deal with the full model or the minimal model in terms of different spin variables. By directly examining the original full model in Eq. (1) and/or the minimal model in Eq. (15), one cannot extract much useful results at least for us. After the proper organization of the active Hilbert space and the definition/introduction of new effective variables, one could then make the connection with the effective transverse field Ising model on the triangular lattice [23, 29, 30]. These procedures are the most insightful parts of this work especially since this is not about constructing models for the expected theoretical results, and luckily the material is organized in such a remarkable way to naturally yield the effective model where the hidden physics can be revealed. The results of the three-sublattice order, BKT physics, 3D XY quantum phase transition, *et al* are all straightforward consequences from these procedures and the observations. Since this is a theoretical work, we can describe our theoretical results with less constraints, and further experiments may make more useful connection.

With the useful results from H_{eff} , we analyze H_{min} with zero field. Since J_0^z is a very high energy scale and

the $\mu_i^z = 1/2$ states are high in energy, the ground state phase diagram is not altered. A bit more careful reasoning could solve H_{min} by separating it into mutually-coupled μ -channel model and τ -channel model, and then obtain the ground states in this Kugel-Khomskii type of mean-field approaches. The μ -channel model gives the ground states with $\mu_i^z = -1/2$ on each site, and the τ -channel model is identical to H_{eff} and thus has the same ground states. This treatment does not involve completely throwing away or projecting out the $\mu_i^z = 1/2$ states and thus does not require a very strong J_0^z .

We then perform the Holstein-Primarkoff spin wave representations for both τ and μ pseudospins. For the three-sublattice ordered state, six Holstein-Primarkoff bosons are introduced. Keeping the quadratic terms in the bosons for the minimal model, we obtain the linear spin-wave model as

$$\begin{aligned}
H_{\text{sw}} &= H_{\text{sw}\tau} + H_{\text{sw}\mu}, \quad (16) \\
H_{\text{sw}\tau} &= \sum_{\mathbf{k}} \sum_{\mu\nu} \left[\mathcal{A}_{\mu\nu}(\mathbf{k}) a_{\mathbf{k}\mu}^\dagger a_{\mathbf{k}\nu} + \mathcal{B}_{\mu\nu}(\mathbf{k}) a_{\mathbf{k}\mu}^\dagger a_{-\mathbf{k}\nu}^{\dagger} \right. \\
&\quad \left. + \mathcal{B}_{\mu\nu}^*(\mathbf{k}) a_{\mathbf{k}\mu} a_{-\mathbf{k}\nu} \right],
\end{aligned}$$

$$H_{\text{sw}\mu} = \sum_{\mathbf{k}} \left[\frac{1}{2} (J_0^z - J_0^\perp \sin \theta) (b_{\mathbf{kA}}^\dagger b_{\mathbf{kA}} + b_{\mathbf{kC}}^\dagger b_{\mathbf{kC}}) + \frac{1}{2} (J_0^z + J_0^\perp) b_{\mathbf{kB}}^\dagger b_{\mathbf{kB}} \right], \quad (17)$$

where \mathbf{k} is summed over the magnetic Brillouin zone, and we have the relation

$$\mathcal{A}_{\mu\nu}(\mathbf{k}) = \mathcal{A}_{\nu\mu}^*(\mathbf{k}), \quad \mathcal{B}_{\mu\nu}(\mathbf{k}) = \mathcal{B}_{\nu\mu}^*(\mathbf{k}). \quad (18)$$

The expressions for \mathcal{A} and \mathcal{B} are listed in the Appendix. In this minimal model, the μ and τ dynamics essentially decouple from each other, and the τ dynamics is identical to the one for the effective model H_{eff} . The full excitations of the three-sublattice ordered state are plotted in Fig. 3(b), as well as the ones at the critical point in Fig. 3(c). With the similar and simpler approaches, we further established the full excitations for the Ising disordered state in Fig. 3(d). The excitations from the μ sectors and the τ sector become separately degenerate in the Ising disordered state.

Discussion.—We have obtained the key properties of the spin model for a dimer triangular lattice antiferromagnet by properly organizing the local spin Hilbert space and defining two new sets of pseudospin variables. The hidden physics of the effective transverse field Ising model is then revealed with these variables. The full model can be thought as the transverse field Ising model of the pseudospin- τ decorated with the pseudospin- μ , and is solved with the mean-field approach and supplied with the existing understanding. In this work, we have mainly dealt with the zero-field case, the characteristic quantum excitations of each quantum phase are established. Although the transformation into the new sets of spin operators makes a great simplification of the problem, the appearance of the original spin operators in the Holstein-Primarkoff bosons becomes rather complex and behaves differently for different spin variables. This naturally involves more than one flavors of Holstein-Primarkoff bosons, and the two-magnon continuum can be induced in the spin correlation. This may cause some complication in the interpretation of the spectroscopic measurement.

Due to the strong Ising anisotropy, the system is expected to support the magnetization plateau. This is realized when the Zeeman energy gain overcomes the dimer singlet formation and the subdominant exchange energy remains optimized or nearly optimized. Unlike the transverse field Ising model on the triangular lattice where the magnetic field simply lifts the degeneracy of the up-up-down and down-down-up spin configurations on the triangular plaquettes and does not alter the Ising exchange, here due to the extra μ -spin degrees of freedom and the bilayer triangular geometry, the polarization of the spin dimer from the singlet to the triplet actually “quenches” the neighboring exchange bonds, generating the emergent lattices. The resulting plateau states are briefly discussed in the appendix. Finally, since our minimal model does not have the fermion sign problem for the

quantum Monte Carlo simulation, we expect more quantitative information to be established in later numerical simulation.

Acknowledgments.—I would like to thank Tong Chen for very recent communication. This work is supported by the National Science Foundation of China with Grant No. 92065203 and by the Ministry of Science and Technology of China with Grants No. 2021YFA1400300.

Appendix A: Mean-field theory for the effective model

This section is devoted to explaining the mean-field treatment for the effective model H_{eff} in the main text. For the three-sublattice ordered state, we introduce the mean-field order parameters in Tab. II. In fact, this assignment of the order parameters captures both the three-sublattice ordered state and the Ising disordered state. When $\theta = -\pi/2$, the system is in the Ising disordered state.

	$\langle \tau_i^z \rangle$	$\langle \tau_i^x \rangle$
$i \in \text{A sublattice}$	$\frac{1}{2} \cos \theta$	$\frac{1}{2} \sin \theta$
$i \in \text{B sublattice}$	0	$-\frac{1}{2}$
$i \in \text{C sublattice}$	$-\frac{1}{2} \cos \theta$	$\frac{1}{2} \sin \theta$

TABLE II. The mean-field order parameters for each sublattices in the three-sublattice ordered phase. Here $\theta < 0$.

In the Weiss mean-field treatment, H_{eff} is reduced to

$$H_{\text{MF}} = \sum_i J_0^\perp \tau_i^x + \sum_{\langle ij \rangle} J_{\text{eff}} \tau_i^z \langle \tau_j^z \rangle \quad (A1)$$

$$= \sum_{i \in \text{A}} [J_0^\perp \tau_i^x - \frac{3}{2} J_{\text{eff}} \cos \theta \tau_i^z] + \sum_{i \in \text{B}} J_0^\perp \tau_i^x + \sum_{i \in \text{C}} [J_0^\perp \tau_i^x + \frac{3}{2} J_{\text{eff}} \cos \theta \tau_i^z], \quad (A2)$$

where all the three sublattices are effectively decoupled. The self-consistent mean-field equations for the A and C sublattices are the same. The self-consistent mean-field equation for the B sublattice is automatically solved as $\tau_i^x = -1/2$. The self-consistent mean-field equation for $i \in \text{A}$ is then given as

$$\langle \tau_i^z \rangle = \frac{\frac{3}{4} J_{\text{eff}} \cos \theta}{[(\frac{3}{2} J_{\text{eff}} \cos \theta)^2 + (J_0^\perp)^2]^{1/2}}, \quad (A3)$$

which yields the critical value of $J_0^\perp / J_{\text{eff}}$ as 1.5. The numerical value was found to be ~ 0.82 [22, 23]. To capture the essential and qualitative physics and be consistent throughout, we stick to the mean-field calculation and explain the quantitative aspect afterwards based on the physical understanding.

Appendix B: Linear spin-wave theory for the effective model

In this section, we perform the linear spin-wave theory to solve for the excitations of the effective model H_{eff} in the three-sublattice ordered state and the Ising disordered state.

1. Three-sublattice ordered state

For both A and C sublattices, the pseudospin vectors point away from x and z directions, and we need to choose the quantization axis to be aligned with the ordered moment in the Holstein-Primarkoff spin wave representation. In the linear spin-wave formulation, the pseudospin operators are represented as

$$\begin{cases} \tau_i^x = +\frac{1}{2} \cos \theta (a_{iA}^\dagger + a_{iA}) + \sin \theta (\frac{1}{2} - a_{iA}^\dagger a_{iA}), \\ \tau_i^z = -\frac{1}{2} \sin \theta (a_{iA}^\dagger + a_{iA}) + \cos \theta (\frac{1}{2} - a_{iA}^\dagger a_{iA}), \end{cases} \quad (\text{B1})$$

for $i \in A$ sublattice,

$$\begin{cases} \tau_i^x = -\frac{1}{2} + a_{iB}^\dagger a_{iB}, \\ \tau_i^z = -\frac{1}{2} (a_{iB}^\dagger + a_{iB}), \end{cases} \quad (\text{B2})$$

for $i \in B$ sublattice, and

$$\begin{cases} \tau_i^x = -\frac{1}{2} \cos \theta (a_{iC}^\dagger + a_{iC}) + \sin \theta (\frac{1}{2} - a_{iC}^\dagger a_{iC}), \\ \tau_i^z = -\frac{1}{2} \sin \theta (a_{iC}^\dagger + a_{iC}) - \cos \theta (\frac{1}{2} - a_{iC}^\dagger a_{iC}), \end{cases} \quad (\text{B3})$$

for $i \in C$ sublattice. According to the specification in Fig. 4, there are three intra-magnetic cell couplings and twelve inter-magnetic cell couplings. Keeping the quadratic terms in the bosons and properly grouping these terms, we obtain the linear spin wave theory,

$$H_{\text{eff}} \rightarrow \sum_{\mathbf{k}} \sum_{\mu\nu} a_{\mathbf{k}\mu}^\dagger a_{\mathbf{k}\nu} \mathcal{A}_{\mu\nu}(\mathbf{k}) + a_{\mathbf{k}\mu}^\dagger a_{-\mathbf{k}\nu}^\dagger \mathcal{B}_{\mu\nu}(\mathbf{k}) + a_{\mathbf{k}\mu}^\dagger a_{-\mathbf{k}\nu}^\dagger \mathcal{B}_{\mu\nu}^*(\mathbf{k}) \quad (\text{B4})$$

where $\mu, \nu = A, B, C$, and the boson hoppings and pairings are given as

$$\mathcal{A}_{11}(\mathbf{k}) = -J_0^\perp \sin \theta + \frac{3}{2} J_{\text{eff}} \cos^2 \theta, \quad (\text{B5})$$

$$\mathcal{A}_{22}(\mathbf{k}) = J_0^\perp, \quad (\text{B6})$$

$$\mathcal{A}_{33}(\mathbf{k}) = -J_0^\perp \sin \theta + \frac{3}{2} J_{\text{eff}} \cos^2 \theta \quad (\text{B7})$$

$$\mathcal{A}_{12}(\mathbf{k}) = \frac{J_{\text{eff}}}{4} \sin \theta (e^{-i\mathbf{k} \cdot \mathbf{a}_1} + e^{-i\mathbf{k} \cdot \mathbf{a}_2} + e^{i\mathbf{k} \cdot \mathbf{a}_3}), \quad (\text{B8})$$

$$\mathcal{A}_{13}(\mathbf{k}) = \frac{J_{\text{eff}}}{4} \sin^2 \theta (e^{i\mathbf{k} \cdot \mathbf{a}_1} + e^{i\mathbf{k} \cdot \mathbf{a}_2} + e^{-i\mathbf{k} \cdot \mathbf{a}_3}), \quad (\text{B9})$$

$$\mathcal{A}_{23}(\mathbf{k}) = \frac{J_{\text{eff}}}{4} \sin \theta (e^{-i\mathbf{k} \cdot \mathbf{a}_1} + e^{-i\mathbf{k} \cdot \mathbf{a}_2} + e^{i\mathbf{k} \cdot \mathbf{a}_3}) \quad (\text{B10})$$

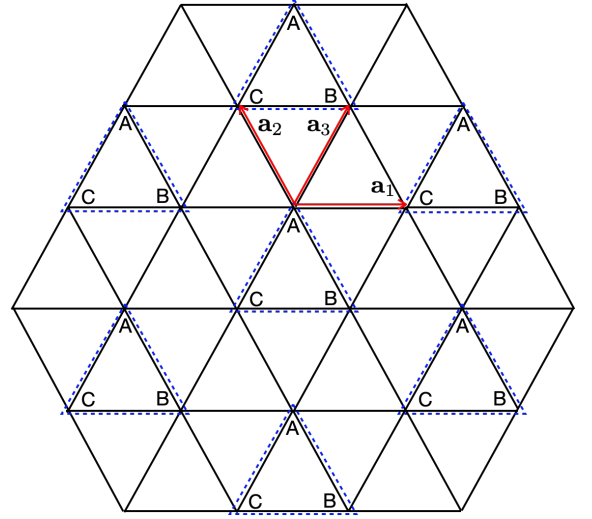


FIG. 4. The specification of magnetic sublattices and magnetic unit cells. The dashed triangle specifies the magnetic unit cell such that the intra- and inter- magnetic unit cell couplings become clear. The vectors $\mathbf{a}_1, \mathbf{a}_2, \mathbf{a}_3$ are three nearest-neighbor vectors of the triangular lattice.

and

$$\mathcal{B}_{12}(\mathbf{k}) = \frac{J_{\text{eff}}}{4} \sin \theta (e^{-i\mathbf{k} \cdot \mathbf{a}_1} + e^{-i\mathbf{k} \cdot \mathbf{a}_2} + e^{i\mathbf{k} \cdot \mathbf{a}_3}) \quad (\text{B11})$$

$$\mathcal{B}_{13}(\mathbf{k}) = \frac{J_{\text{eff}}}{4} \sin^2 \theta (e^{i\mathbf{k} \cdot \mathbf{a}_1} + e^{i\mathbf{k} \cdot \mathbf{a}_2} + e^{-i\mathbf{k} \cdot \mathbf{a}_3}), \quad (\text{B12})$$

$$\mathcal{B}_{23}(\mathbf{k}) = \frac{J_{\text{eff}}}{4} \sin \theta (e^{-i\mathbf{k} \cdot \mathbf{a}_1} + e^{-i\mathbf{k} \cdot \mathbf{a}_2} + e^{i\mathbf{k} \cdot \mathbf{a}_3}) \quad (\text{B13})$$

2. Ising disordered state

For the Ising disordered state, there is only one sublattice, and the spin-wave representation is much simpler and is given as

$$\begin{cases} \tau_i^x = -\frac{1}{2} + a_i^\dagger a_i, \\ \tau_i^z = -\frac{1}{2} (a_i^\dagger + a_i), \end{cases} \quad (\text{B14})$$

and the linear spin-wave Hamiltonian is then obtained as

$$H_{\text{eff}} \rightarrow \frac{J_{\text{eff}}}{4} \sum_{\mathbf{k}} \sum_{\mu} \cos(\mathbf{k} \cdot \mathbf{a}_\mu) (a_{\mathbf{k}} a_{-\mathbf{k}} + a_{\mathbf{k}}^\dagger a_{-\mathbf{k}}^\dagger + 2a_{\mathbf{k}}^\dagger a_{\mathbf{k}}) + J_0^\perp \sum_{\mathbf{k}} a_{\mathbf{k}}^\dagger a_{\mathbf{k}}, \quad (\text{B15})$$

where the momentum summation is over the Brillouin zone of the triangular lattice. The excitation spectrum is ready to be solved and is given as

$$\epsilon_{\mathbf{k}} = 2 \left[\left(\sum_{\mu} \frac{1}{4} J_{\text{eff}} \cos(\mathbf{k} \cdot \mathbf{a}_\mu) + \frac{1}{2} J_0^\perp \right)^2 \right]$$

$$-\left(\sum_{\mu} \frac{1}{4} J_{\text{eff}} \cos(\mathbf{k} \cdot \mathbf{a}_{\mu})\right)^2\right]^{1/2}. \quad (\text{B16})$$

The dispersion arises from the effective exchange J_{eff} , and becomes flat when $J_{\text{eff}} \rightarrow 0$.

Appendix C: Mean-field theory for the minimal model

We extend the mean-field treatment for the effective model H_{eff} to the minimal model H_{min} . This mean-field treatment requires extra steps. One can actually adopt some experiences from the Kugel-Khomskii spin-orbital exchange model where one can decouple the full model into the mutually-dependent spin and orbital mean-field models. Here, we decouple the minimal model H_{min} with coupled pseudospin τ_i and μ_j into the mutually-dependent mean-field models, and the models are given as

$$H_{\mu\text{MF}} = \sum_i \frac{1}{2} J_0^z \mu_i^z + J_0^{\perp} \langle \tau_i^x \rangle \left(\frac{1}{2} - \mu_i^z \right) + \sum_{\langle ij \rangle} \langle \tau_i^z \tau_j^z \rangle \times [J_1^z (1 + 4\mu_i^z \mu_j^z) + 2J_2^z (\mu_i^z + \mu_j^z)], \quad (\text{C1})$$

$$H_{\tau\text{MF}} = \sum_i J_0^{\perp} \tau_i^x \left[\frac{1}{2} - \langle \mu_i^z \rangle \right] + \sum_{\langle ij \rangle} \tau_i^z \tau_j^z \times [J_1^z (1 + 4\langle \mu_i^z \mu_j^z \rangle) + 2J_2^z (\langle \mu_i^z \rangle + \langle \mu_j^z \rangle)] \quad (\text{C2})$$

Since J_0^z is the dominant energy scale, $H_{\mu\text{MF}}$ can be viewed as the Ising model with non-uniform Ising couplings in a strong “magnetic field”. The Ising coupling depends on the bond correlation $\langle \tau_i^z \tau_j^z \rangle$. $H_{\tau\text{MF}}$ should be viewed as a transverse field Ising model with the bond-dependent exchange couplings and site-dependent local transverse field.

Here we explain that μ_i^z should be polarized to $-1/2$. First of all, a strong “magnetic field” of J_0^z should already be sufficient to polarize the pseudospin μ_i^z as $\mu_i^z = -1/2$. Nevertheless, one can further soften the condition. From $H_{\tau\text{MF}}$, the effective transverse field on τ^x is always positive. This is due to the fact that

$$\frac{1}{2} - \langle \mu_i^z \rangle > 0. \quad (\text{C3})$$

The extreme case with $\mu_i^z = 1/2$ cannot happen as it is disfavored by a large J_0^z . Thus we have $\langle \tau_i^x \rangle < 0$ throughout. In order to optimize the second term alone in $H_{\mu\text{MF}}$, we should require $\mu_i^z = -1/2$. The analysis of the third term in $H_{\mu\text{MF}}$ requires the knowledge of $\langle \tau_i^z \tau_j^z \rangle$ that can be considered from $H_{\tau\text{MF}}$. Although a strong J_0^z would be sufficient to force $\langle \mu_i^z \rangle = -1/2$, since we are now softening this condition, a not-so-strong J_0^z would simply favor a uniform $\langle \mu_i^z \rangle < 0$ with the support of the second term in $H_{\mu\text{MF}}$. This indicates that

$$\begin{cases} J_1^z [1 + 4\langle \mu_i^z \mu_j^z \rangle] > J_1^z, \\ -2J_2^z \leq 2J_2^z [\langle \mu_i^z \rangle + \langle \mu_j^z \rangle] < 0. \end{cases} \quad (\text{C4})$$

From the exchange path and distances, it is expected that $J_1^z \gg J_2^z$. Thus, $H_{\tau\text{MF}}$ is the transverse field Ising model with the antiferromagnetic exchange, and this generally favors $\langle \tau_i^z \tau_j^z \rangle < 0$. Thus, in the third term of $H_{\mu\text{MF}}$, the exchange coupling is ferromagnetic, and the overall coefficient of the J_2 term is ferromagnetic. Since J_2 is small, it cannot flip the sign of the total effective magnetic field for μ_i^z . Thus, one can safely conclude that

$$\mu_i^z = -\frac{1}{2}. \quad (\text{C5})$$

for all sites even if the dominant energy scale J_0^z is reduced.

With Eq. (C5), the mean-field model $H_{\tau\text{MF}}$ immediately becomes H_{eff} . Alternatively, one could simply set $\mu_i^z = -1/2$ in the original minimal model H_{min} . The outcome is the same. But to obtain this outcome, one has to go through the above explanation.

Appendix D: Linear spin-wave theory for the minimal model

Since the pseudospin $\mu_i^z = -1/2$ throughout the parameter regime of our interest, the Holstein-Primarkoff boson representation is the same in both three-sublattice ordered state and the Ising disordered state for the minimal model. We replace the pseudospin operator μ_i as

$$\mu_i^z = -\frac{1}{2} + b_i^{\dagger} b_i, \quad (\text{D1})$$

and there is no other transverse component involved in H_{min} . For the full model with finite J_1^{\perp} and J_2^{\perp} , the transverse components are needed.

1. Three sublattice order in the minimal model

For the three-sublattice ordered state, the τ -spins are represented in the same way as prescribed in Sec. B1. As the transverse component of μ spins is not involved in H_{min} , no dispersion is created. The resulting linear spin-wave model for the three-sublattice order is given as

$$H_{\text{sw}} = H_{\text{sw}\tau} + H_{\text{sw}\mu}, \quad (\text{D2})$$

where $H_{\text{sw}\tau}$ is identical to the one in Sec. B1, and $H_{\text{sw}\mu}$ is given as

$$H_{\text{sw}\mu} = \sum_{\mathbf{k}} \left[\frac{1}{2} (J_0^z - J_0^{\perp} \sin \theta) (b_{\mathbf{kA}}^{\dagger} b_{\mathbf{kA}} + b_{\mathbf{kC}}^{\dagger} b_{\mathbf{kC}}) + \frac{1}{2} (J_0^z + J_0^{\perp}) b_{\mathbf{kB}}^{\dagger} b_{\mathbf{kB}} \right], \quad (\text{D3})$$

where the summation of the momentum is over the magnetic Brillouin zone. This creates three flat bands of μ -sector excitations on top of the τ -sector excitations. Among these three flat bands, two are degenerate.

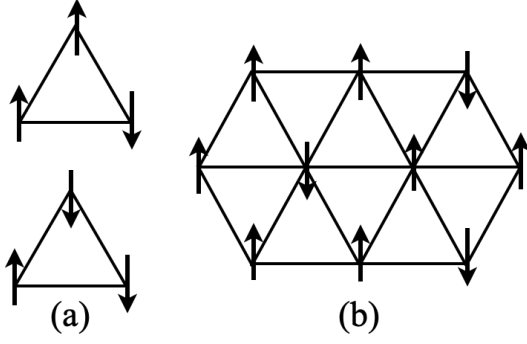


FIG. 5. (a) The degenerate up-up-down and down-down-up spin configurations for the classical Ising model on the triangular plaquette. (b) The 1/3 magnetization plateau state on the triangular lattice.

2. Ising disordered state in the minimal model

For the Ising disordered state, the τ component is represented in the same way as the expression in Eq. (B14), and the minimal model is reduced to the spin wave model as

$$H_{\min} \rightarrow \frac{J_{\text{eff}}}{4} \sum_{\mathbf{k}} \sum_{\mu} \cos(\mathbf{k} \cdot \mathbf{a}_{\mu}) (a_{\mathbf{k}} a_{-\mathbf{k}} + a_{\mathbf{k}}^{\dagger} a_{-\mathbf{k}}^{\dagger} + 2a_{\mathbf{k}}^{\dagger} a_{\mathbf{k}}) + \sum_{\mathbf{k}} J_0^{\perp} a_{\mathbf{k}}^{\dagger} a_{\mathbf{k}} + \sum_{\mathbf{k}} \frac{1}{2} (J_0^z + J_0^{\perp}) b_{\mathbf{k}}^{\dagger} b_{\mathbf{k}}, \quad (\text{D4})$$

where a flat excitation of the μ sector with the energy $\frac{1}{2}(J_0^z + J_0^{\perp})$ is introduced on top of the excitation of the effective model H_{eff} .

Appendix E: Magnetization plateau states

Here we give a discussion of the magnetization plateau states in the presence of z -direction magnetic fields. To motivate this discussion, we first sketch the 1/3 magnetization plateau state for the antiferromagnetic Ising model on the triangular lattice under the external magnetic field on the Ising component. The Zeeman coupling over there immediately lifts the degeneracy of the “down-down-up” and “up-up-down” spin configurations for each triangular plaquette (see Fig. 5(a)). Once the “up-up-down” spin configuration is fixed on one triangular plaquette, the spin configuration on the whole triangular lattice is determined (see Fig. 5(b)), and the exchange energy on each triangular plaquette is optimized. Such a “up-up-down” state retains the three-sublattice structure and gives rise to the 1/3 magnetization plateau on the triangular lattice. Due to the robustness of this “up-up-down” state, it persists even to the quantum case with the transverse field [23].

For the minimal model H_{\min} , the local Hilbert space is large, and this is where the complication and difference arise. We consider the classical limit by setting $J_0^{\perp} = 0$,

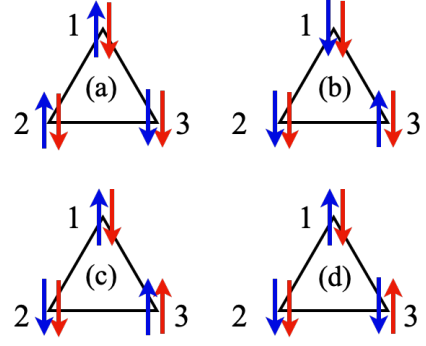


FIG. 6. (a) and (b) are the τ^z Ising spin configurations with $\mu_i^z = -1/2$ throughout on one triangular plaquette. (c) and (d) are the τ^z Ising spin configurations by flipping one μ_i^z from $-1/2$ to $+1/2$. The blue arrows are for τ^z spins, and the red arrows are for μ^z spins. The same choice is given for the other figures.

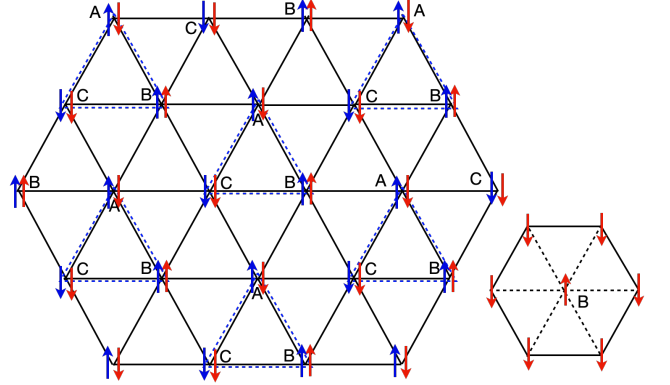


FIG. 7. The spin configuration for the 1/3 magnetization plateau of the minimal model by setting $J_0^{\perp} = 0$. The B sublattice has $\mu_i^z = 1/2$. In the inset, the dashed bonds have zero exchange coupling for τ^z 's, and the remaining hexagon with even number of bonds is antiferromagnetically coupled for the τ^z spins.

and the regime with $J_0^z \gg J_1^z \gg J_2^z$. At the zero magnetic field, $\mu^z = -1/2$ on every site, and the model is the antiferromagnetic Ising model with τ variables. For each triangular plaquette, there exist one unsatisfied bond and two satisfied bonds, and overall there is one net satisfied bonds for the Ising spin interactions of the τ spins. This is shown as Figs. 6(a) and (b). When the external magnetic field polarizes one dimer singlet into the dimer triplet by flipping one μ_i^z from $-1/2$ to $+1/2$, the exchange coupling on the antiferromagnetically arranged μ^z bond is quenched. In Figs. 6(c) and (d), the exchange interactions on the 13 and 23 bonds are zero, and the remaining 23 bond is optimized. Thus, the net satisfied bond on the triangular plaquette remains to be one. The spin state in Fig. 6(d) does not gain Zeeman energy for the positive- z magnetic field compared to the spin state in Fig. 6(c) because the total magnetization on the site 3 is down. Once the Zeeman energy gain of the spin state in

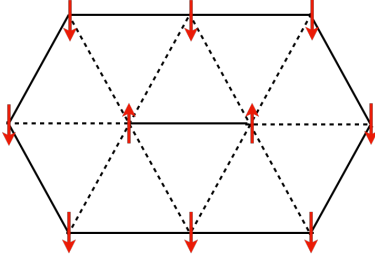


FIG. 8. The dashed bonds have zero exchange coupling for τ^z 's, and the remaining stretched hexagon with even number of bonds is antiferromagnetically coupled for the τ^z spins. The two central sites have $\mu^z = 1/2, \tau^z = 1/2$ to gain the Zeeman energy.

Fig. 6(c) overcomes the singlet-triplet energy gap $J_0^z/2$, then the spin state is satisfied. To make sure only one μ_i^z spin to be flipped for each triangular plaquette for the whole triangular lattice, one arrange the $\mu^z = 1/2$ sites in a next-nearest neighbor fashion, which is very much like the “up” spin of the $1/3$ magnetization state in Fig. 5(b). As we show in Fig. 7, the B sites have $\mu^z = 1/2, \tau_i^z = 1/2$ to gain the Zeeman energy, and are decoupled from the remaining sites due to the quenched exchange interactions. The remaining sites have $\mu^z = -1/2$ and form an emergent honeycomb lattice that are unfrustrated (see the inset of Fig. 7). These sites have an antiferromagnetically arranged τ^z spin configuration, and there is no extensive or subextensive degeneracy any more. The magnetization of this state is solely contributed from the B sites and is equal to $1/3$ of the fully polarized state. Due to the robustness of this state, the system should have the $1/3$ magnetization plateau for this state. As it is depicted in Fig. 7, this state retains the three-sublattice structure.

If one further increases the magnetic field, more μ^z

spins will be flipped, and this will necessarily generate the case with the neighboring $\mu^z = +1/2$ bond. As we depict in Fig. 8, the bond with $\mu^z = +1/2$ is decoupled from all other neighboring sites on the dashed bonds due to the quenched exchange couplings, and the exchange energy of the central bond is enhanced as well. The Zeeman energy of two central sites in Fig. 8 has to overcome both the singlet-triplet energy of two sites and the exchange energy cost. The stretched hexagon has even number of sites and has the τ^z -spin antiferromagnetically arranged. If one arranges the stretched hexagons on the triangular lattice, the resulting state has a magnetization plateau that is equal to $1/2$ of the fully polarized state. With even stronger magnetic fields, one could continue this procedure to construct more plateau states.

Appendix F: The spin components in the spin-wave bosons

In the main text and Sec. B 1, we have already seen that, the τ^z - τ^z correlation should contain both the single-magnon excitation and the two-magnon continuum. Based on Tab. I, one could express each spin component in terms of the Holstein-Primarkoff bosons for τ and μ pseudospins. The spin components S_{ui}^z and S_{di}^z correspond to $+\tau_i^z$ and $-\tau_i^z$ for the zero-field ground state, respectively. We here work out the total spin operators for each dimer in terms of the spin-wave bosons. They are listed as follows,

$$S_{ui}^z + S_{di}^z = \tau_i^z(1 + 2\mu_i^z), \quad (F1)$$

$$S_{ui}^x + S_{di}^x = (2\tau_i^x + 1)\mu_i^x, \quad (F2)$$

$$S_{ui}^y + S_{di}^y = 2\tau_i^y\mu_i^x + 2\tau_i^z\mu_i^y, \quad (F3)$$

and most of these relations are not linear, and thus various complication will arise.

For the Ising disordered state at the zero field, it is straightforward to express them in terms of the spin-wave bosons, and we have

$$S_{ui}^z + S_{di}^z = -[(1 - a_i^\dagger a_i)^{\frac{1}{2}} a_i + a_i^\dagger (1 - a_i^\dagger a_i)^{\frac{1}{2}}] b_i^\dagger b_i \simeq -(a_i + a_i^\dagger) b_i^\dagger b_i, \quad (F4)$$

$$\begin{aligned} S_{ui}^x + S_{di}^x &= (-1 + 2a_i^\dagger a_i) \frac{1}{2} [(1 - b_i^\dagger b_i)^{\frac{1}{2}} b_i + b_i^\dagger (1 - b_i^\dagger b_i)^{\frac{1}{2}}] \simeq \frac{1}{2} (-1 + 2a_i^\dagger a_i) (b_i + b_i^\dagger) \\ &= -\frac{1}{2} (b_i + b_i^\dagger) + a_i^\dagger a_i (b_i + b_i^\dagger), \end{aligned} \quad (F5)$$

$$\begin{aligned} S_{ui}^y + S_{di}^y &= 2 \times \frac{a_i^\dagger (1 - a_i^\dagger a_i)^{\frac{1}{2}} - (1 - a_i^\dagger a_i)^{\frac{1}{2}} a_i}{2i} \times \frac{(1 - b_i^\dagger b_i)^{\frac{1}{2}} b_i + b_i^\dagger (1 - b_i^\dagger b_i)^{\frac{1}{2}}}{2} \\ &\quad + 2 \times \frac{(1 - a_i^\dagger a_i)^{\frac{1}{2}} a_i + a_i^\dagger (1 - a_i^\dagger a_i)^{\frac{1}{2}}}{-2} \times \frac{b_i^\dagger (1 - b_i^\dagger b_i)^{\frac{1}{2}} - (1 - b_i^\dagger b_i)^{\frac{1}{2}} b_i}{2i} \\ &\simeq i(a_i b_i^\dagger - a_i^\dagger b_i), \end{aligned} \quad (F6)$$

where “ \simeq ” refers to the linear order approximation for the spin-wave boson of each pseudospin. At this linear order, only “ $S_{ui}^x + S_{di}^x$ ” involves the linear spin-wave boson b_i and b_i^\dagger , and all others involve more than one flavors of the boson operators. The relation of the dynamic spin correlations with the elementary excitations requires a bit scrutiny.

For the three-sublattice order at the zero field, the expression of the spin operators in terms of the spin-wave bosons depends on the magnetic sublattice. For the A sublattice, we have

$$\begin{aligned} S_{ui}^z + S_{di}^z &= \left[-\frac{1}{2} \sin \theta (a_{iA}^\dagger \sqrt{1 - a_{iA}^\dagger a_{iA}} + \sqrt{1 - a_{iA}^\dagger a_{iA}} a_{iA}) + \cos \theta \left(\frac{1}{2} - a_{iA}^\dagger a_{iA} \right) \right] (2b_{iA}^\dagger b_{iA}) \\ &\simeq [-\sin \theta (a_{iA}^\dagger + a_{iA}) + \cos \theta] b_{iA}^\dagger b_{iA}, \end{aligned} \quad (\text{F7})$$

$$\begin{aligned} S_{ui}^x + S_{di}^x &= \left[\frac{1}{2} \cos \theta (a_{iA}^\dagger \sqrt{1 - a_{iA}^\dagger a_{iA}} + \sqrt{1 - a_{iA}^\dagger a_{iA}} a_{iA}) + \sin \theta \left(\frac{1}{2} - a_{iA}^\dagger a_{iA} \right) \right] \frac{1}{2} [(1 - b_{iA}^\dagger b_{iA})^{\frac{1}{2}} b_{iA} + b_{iA}^\dagger (1 - b_{iA}^\dagger b_{iA})^{\frac{1}{2}}] \\ &\simeq \frac{1}{4} \cos \theta (a_{iA}^\dagger + a_{iA}) (b_{iA} + b_{iA}^\dagger) + \frac{1}{2} \sin \theta \left(\frac{1}{2} - a_{iA}^\dagger a_{iA} \right) (b_{iA} + b_{iA}^\dagger), \end{aligned} \quad (\text{F8})$$

$$\begin{aligned} S_{ui}^y + S_{di}^y &= 2 \times \frac{\sqrt{1 - a_{iA}^\dagger a_{iA}} a_{iA} - a_{iA}^\dagger \sqrt{1 - a_{iA}^\dagger a_{iA}}}{2i} \times \frac{(1 - b_{iA}^\dagger b_{iA})^{\frac{1}{2}} b_{iA} + b_{iA}^\dagger (1 - b_{iA}^\dagger b_{iA})^{\frac{1}{2}}}{2} \\ &\quad + 2 \times \left[-\frac{1}{2} \sin \theta (a_{iA}^\dagger + a_{iA}) + \cos \theta \left(\frac{1}{2} - a_{iA}^\dagger a_{iA} \right) \right] \times \frac{1}{2i} [b_{iA}^\dagger (1 - b_{iA}^\dagger b_{iA})^{\frac{1}{2}} - (1 - b_{iA}^\dagger b_{iA})^{\frac{1}{2}} b_{iA}] \\ &\simeq \frac{-i}{2} (a_{iA} - a_{iA}^\dagger) (b_{iA} + b_{iA}^\dagger) + \frac{i \sin \theta}{2} (a_{iA} + a_{iA}^\dagger) (b_{iA}^\dagger - b_{iA}) + \frac{-i \cos \theta}{2} (b_{iA}^\dagger - b_{iA}). \end{aligned} \quad (\text{F9})$$

Likewise, for the C sublattice, the expression is obtained by setting $\theta \rightarrow \pi - \theta$ and $A \rightarrow C$. For the B sublattice, the expression is obtained by setting $\theta \rightarrow -\pi/2$ and $A \rightarrow B$.

-
- [1] C. Lacroix, P. Mendels, and F. Mila, *Introduction to Frustrated Magnetism: Materials, Experiments, Theory* (2011).
- [2] W. Witczak-Krempa, G. Chen, Y. B. Kim, and L. Balents, Correlated Quantum Phenomena in the Strong Spin-Orbit Regime, *Annual Review of Condensed Matter Physics* **5**, 57–82 (2014).
- [3] H. Takagi, T. Takayama, G. Jackeli, G. Khaliullin, and S. E. Nagler, Concept and realization of Kitaev quantum spin liquids, *Nature Reviews Physics* **1**, 264–280 (2019).
- [4] J. G. Rau and M. J. Gingras, Frustrated Quantum Rare-Earth Pyrochlores, *Annual Review of Condensed Matter Physics* **10**, 357–386 (2019).
- [5] H. Liu and G. Khaliullin, Pseudospin exchange interactions in d^7 cobalt compounds: Possible realization of the Kitaev model, *Phys. Rev. B* **97**, 014407 (2018).
- [6] R. Sano, Y. Kato, and Y. Motome, Kitaev-Heisenberg Hamiltonian for high-spin d^7 Mott insulators, *Phys. Rev. B* **97**, 014408 (2018).
- [7] R. Coldea, D. A. Tennant, E. M. Wheeler, E. Wawrzynska, D. Prabhakaran, M. Telling, K. Habicht, P. Smeibidl, and K. Kiefer, Quantum Criticality in an Ising Chain: Experimental Evidence for Emergent E_8 Symmetry, *Science* **327**, 177–180 (2010).
- [8] A. W. Kinross, M. Fu, T. J. Munsie, H. A. Dabkowska, G. M. Luke, S. Sachdev, and T. Imai, Evolution of Quantum Fluctuations Near the Quantum Critical Point of the Transverse Field Ising Chain System CoNb_2O_6 , *Phys. Rev. X* **4**, 031008 (2014).
- [9] C. M. Morris, N. Desai, J. Viirok, D. H  vonen, U. Nagel, T. R   m, J. W. Krizan, R. J. Cava, T. M. McQueen, S. M. Koohpayeh, R. K. Kaul, and N. P. Armitage, Duality and domain wall dynamics in a twisted Kitaev chain, *Nature Physics* **17**, 832–836 (2021).
- [10] Z. Wang, T. Lorenz, D. I. Gorbunov, P. T. Cong, Y. Kohama, S. Niesen, O. Breunig, J. Engelmayr, A. Herman, J. Wu, K. Kindo, J. Wosnitza, S. Zherlitsyn, and A. Loidl, Quantum Criticality of an Ising-like Spin-1/2 Antiferromagnetic Chain in a Transverse Magnetic Field, *Phys. Rev. Lett.* **120**, 207205 (2018).
- [11] S. Suga, Tomonaga–Luttinger Liquid in Quasi-One-Dimensional Antiferromagnet $\text{BaCo}_2\text{V}_2\text{O}_8$ in Magnetic Fields, *Journal of the Physical Society of Japan* **77**, 074717 (2008).
- [12] Z. Wang, J. Wu, W. Yang, A. K. Bera, D. Kamenskyi, A. T. M. N. Islam, S. Xu, J. M. Law, B. Lake, C. Wu, and A. Loidl, Experimental observation of Bethe strings, *Nature* **554**, 219–223 (2018).
- [13] Y. Cui, H. Zou, N. Xi, Z. He, Y. X. Yang, L. Shu, G. H. Zhang, Z. Hu, T. Chen, R. Yu, J. Wu, and W. Yu, Quantum Criticality of the Ising-like Screw Chain Antiferromagnet $\text{SrCo}_2\text{V}_2\text{O}_8$ in a Transverse Magnetic Field, *Phys. Rev. Lett.* **123**, 067203 (2019).
- [14] H. Zou, Y. Cui, X. Wang, Z. Zhang, J. Yang, G. Xu, A. Okutani, M. Hagiwara, M. Matsuda, G. Wang, G. Mussardo, K. H  ds  gi, M. Kormos, Z. He, S. Kimura, R. Yu, W. Yu, J. Ma, and J. Wu, E_8 Spectra of Quasi-One-Dimensional Antiferromagnet $\text{BaCo}_2\text{V}_2\text{O}_8$ under Transverse Field, *Phys. Rev. Lett.* **127**, 077201 (2021).
- [15] R. Zhong, S. Guo, L. T. Nguyen, and R. J. Cava, Frustrated spin-1/2 dimer compound $\text{K}_2\text{Co}_2(\text{SeO}_3)_3$ with easy-axis anisotropy, *Phys. Rev. B* **102**, 224430 (2020).
- [16] J. Sheng, L. Wang, A. Candini, W. Jiang, L. Huang, B. Xi, J. Zhao, H. Ge, N. Zhao, Y. Fu, J. Ren, J. Yang, P. Miao, X. Tong, D. Yu, S. Wang, Q. Liu, M. Kofu, R. Mole, G. Biasiol, D. Yu, I. A. Zaliznyak, J.-W. Mei, and L. Wu, Two-dimensional quantum universality in the spin-1/2 triangular-lattice quantum antiferromagnet $\text{Na}_2\text{BaCo}(\text{PO}_4)_2$, *Proceedings of the National Academy of Sciences* **119**, e2211193119 (2022).

- [17] J. Xiang, C. Zhang, Y. Gao, W. Schmidt, K. Schmalzl, C.-W. Lu, B. Li, N. Xi, X.-Y. Liu, H. Jin, G. Li, J. Shen, Z. Chen, Y. Qi, Y. Wan, W. Jin, W. Li, P. Sun, and G. Su, Giant magnetocaloric effect in spin supersolid candidate $\text{Na}_2\text{BaCo}(\text{PO}_4)_2$, *Nature* **625**, 270 (2024).
- [18] H. Jia, B. Ma, Z. Wang, and G. Chen, Quantum spin supersolid as a precursory dirac spin liquid in a triangular lattice antiferromagnet (2023), [arXiv:2304.11716 \[cond-mat.str-el\]](#).
- [19] J. Ma, Y. Kamiya, T. Hong, H. B. Cao, G. Ehlers, W. Tian, C. D. Batista, Z. L. Dun, H. D. Zhou, and M. Matsuda, Static and Dynamical Properties of the Spin-1/2 Equilateral Triangular-Lattice Antiferromagnet $\text{Ba}_3\text{CoSb}_2\text{O}_9$, *Phys. Rev. Lett.* **116**, 087201 (2016).
- [20] R. Moessner and S. L. Sondhi, Ising models of quantum frustration, *Phys. Rev. B* **63**, 224401 (2001).
- [21] G. Chen, Intrinsic transverse field in frustrated quantum ising magnets: Physical origin and quantum effects, *Phys. Rev. Res.* **1**, 033141 (2019).
- [22] S. V. Isakov and R. Moessner, Interplay of quantum and thermal fluctuations in a frustrated magnet, *Phys. Rev. B* **68**, 104409 (2003).
- [23] C. Liu, C.-J. Huang, and G. Chen, Intrinsic quantum Ising model on a triangular lattice magnet TmMgGaO_4 , *Phys. Rev. Res.* **2**, 043013 (2020).
- [24] J. V. José, L. P. Kadanoff, S. Kirkpatrick, and D. R. Nelson, Renormalization, vortices, and symmetry-breaking perturbations in the two-dimensional planar model, *Phys. Rev. B* **16**, 1217 (1977).
- [25] K. Damle, Melting of Three-Sublattice Order in Easy-Axis Antiferromagnets on Triangular and Kagome Lattices, *Phys. Rev. Lett.* **115**, 127204 (2015).
- [26] S. Biswas and K. Damle, Singular ferromagnetic susceptibility of the transverse-field Ising antiferromagnet on the triangular lattice, *Phys. Rev. B* **97**, 085114 (2018).
- [27] F. Mila, Low-Energy Sector of the $S = 1/2$ Kagome Antiferromagnet, *Phys. Rev. Lett.* **81**, 2356 (1998).
- [28] G. Chen and C. Wu, Multiflavor mott insulators in quantum materials and ultracold atoms, *npj Quantum Materials* **9**, 1 (2021).
- [29] Y. Shen, C. Liu, Y. Qin, S. Shen, Y.-D. Li, R. Bewley, A. Schneidewind, G. Chen, and J. Zhao, Intertwined dipolar and multipolar order in the triangular-lattice magnet TmMgGaO_4 , *Nature Communications* **10**, 10.1038/s41467-019-12410-3 (2019).
- [30] J. c. v. Chaloupka, Emergent transverse-field Ising model in d^4 spin-orbit Mott insulators, *Phys. Rev. B* **109**, L020403 (2024).